Journal of Molecular Liquids 311 (2020) 113340

Contents lists available at ScienceDirect

Journal of Molecular Liquids

journal homepage: www.elsevier.com/locate/molliq

# Vibrational spectrum of 1-ethyl-3-methylimidazolium tetrafluoroborate on graphene surface

Jiao Zhang [a,1], Yongji Guan [a,1], Jinyuan Wang [c], Fulong Yang [d], Huanwang Jing [c], Xiaoping Zhang [a,*], Youquan Deng [b,*]

[a] Institute of Optoelectronics and Electromagnetic Information, School of Information Science and Engineering, Lanzhou University, Lanzhou 730000, China
[b] Centre for Green Chemistry and Catalysis, Lanzhou Institute of Chemical Physics, Chinese Academy of Sciences, Lanzhou 730000, China
[c] State Key Laboratory of Applied Organic Chemistry, College of Chemistry and Chemical Engineering, Lanzhou University, Lanzhou 730000, China
[d] College of Electrical and Information Engineering, Lanzhou University of Technology, Lanzhou 730050, China

ARTICLE INFO

*Article history:*
Received 7 January 2020
Received in revised form 6 May 2020
Accepted 8 May 2020
Available online 15 May 2020

*Keywords:*
Vibrational spectrum
Ionic liquid
Interface
Density functional theory

ABSTRACT

Ionic liquids (ILs) are promising novel solvents for energy harvesting and understanding the graphene/ILs interface structural characteristics is required. In this study, we calculate the vibrational spectrum (VS) of 1-ethyl-3-methylimidazolium tetrafluoroborate ([Emim][$BF_4$]) pair on graphene surface in the range from 10 to 3500 $cm^{-1}$ and systemically investigate the influence of the graphene on the VS of [Emim][$BF_4$] using density functional theory. The results show 24 vibrational bands (VBs) with obvious shifting. The VBs at 3170.26 and 3033.51 $cm^{-1}$ show a redshift of 59.46 and 14.95 $cm^{-1}$ respectively which was mainly caused by the enhanced hydrogen bond strength of C2—H···F and F atoms with the C—H on the ethyl chain. The VBs at 101.49 and 1417.43 $cm^{-1}$ show a blueshift of 62.43 and 23.86 $cm^{-1}$ due to the enhancement of induction effect of [Emim][$BF_4$] on graphene surface (from −44.68 to −45.42 kJ $mol^{-1}$). The VB at 86.91 $cm^{-1}$ shows a redshift of 59.43 $cm^{-1}$ which can be ascribed to the reduction of the whole interaction energy between the cation and anion of [Emim][$BF_4$] on graphene surface (from −367.06 to −356.06 kJ·$mol^{-1}$). Overall, these shifts of the VS are mainly attributed to the attraction between graphene and anion $[BF_4]^-$, which is dominated by the induction and dispersion interaction accounting for 63.43% and 34.37% of the attraction interaction respectively. Due to this attraction, the anion $[BF_4]^-$ move closer to the surface of graphene.



## 1. Introduction

The vibrational spectrum (VS), also known as infrared absorption spectrum, is produced by the transition between different vibrational energy levels or rotational energy levels in the same electron energy state in the molecule due to the selective absorption of certain wavelengths of infrared by molecules. VS is a multifunctional tool to display the structural characteristics of solid and liquid materials or their solutions, such as conformation functional groups and hydrogen bonds (HBs). The previous research on vibrational spectra mainly focused on the experimental [1] and computational simulation of water [2,3]. Falk and co-works [1] have studied the VS of hydrogen-deuterium-oxygen (HDO) at low concentrations in $H_2O$ and in $D_2O$ between 0° and 130° used a double-beam technique. Silvestrelli and co-workers [2] investigated the infrared spectrum of liquid water with Car-Parrinello molecular dynamics (MD) using ab initio calculation and evaluated the electronic polarization by means of the Berry phase formulation. The major features of the spectrum are in good agreement with experiments, indicating the accuracy of the quantum-correction simulation approach in describing the properties of liquid water under ambient conditions. Zhang et al. [3] performed a first principles hybrid functional simulation of liquid water to yield a much better agreement with experimental results than a semi-local functional description. In particular, the calculated stretching and bending bands are in good agreement with experimental VS.

ILs are a series of novel liquids solely composed of bulky organic cations and organic or inorganic anions [4,5]. Their excellent properties include low melting point, negligible vapor pressure, wide electrochemical window, wide liquid range, recyclability, nonflammability, and thermal/chemical stability [6–13]. These excellent properties render ILs to be a very useful medium for liquid/liquid extraction, electrochemistry, chemical syntheses and catalysis [14–16]. In recent years, ILs have also been widely applied in lab on a chip [17], variable-focus lenses [18], flow-induced energy harvesting [19–22] and electrowetting [23,24]. As environmentally friendly solvents, ILs have been attracted much theoretical interest for broad applications in chemical

* Corresponding authors.
*E-mail addresses:* zxp@lzu.edu.cn (X. Zhang), ydeng@licp.cas.cn (Y. Deng).
[1] These authors contributed equally to this work.

https://doi.org/10.1016/j.molliq.2020.113340
0167-7322/

and industrial processes, so atomic understanding of the physicochemical properties and structures of ILs is essential vast majority of these applications. Fumino et al. [25] investigated the cation-anion and cation-solvent interactions in solutions of the protic ionic liquid (PIL) tetraethylammonium iodide ([$Et_3NH$][I]) dissolved in solvents of different polarities by means of far infrared vibrational (FIR) spectroscopy and density functional theory (DFT) calculations. They found that for these PIL-solvent mixtures, the position of the vibrational peak of interaction between cation and anion of the contact ion pairs (CIPs) are reformed by increasing the temperature due to the reduced polarity of the solvent. Velpula and co-workers [26] performed Raman experiments and MD simulation to investigate the graphene with a series of 1-alkyl-3-methylimidazolium tetrafluoroborate ionic liquids ([$C_n$mim][$BF_4$]) interface at room temperature (21–23 °C). They found that n-type doping of graphene originates from the changes in the electrostatic potential at the graphene/IL interface, and the magnitude of doping increases with increasing cation chain length. Pensado et al. [27] investigated the interfacial layer structure of the ionic liquid 1-ethyl-3-methylimidazolium thiocyanate ([Emim][SCN]) at a flat graphene surface and inside of single-wall carbon nanotubes of different diameters. They found that an ordered layer of ions formed at the graphene/ILs interface which is essentially one ion thick.

It is worth exploring that ionic liquids are being used as electrolyte materials [28,29] as promising candidates in the next generation of supercapacitors, whose performance requires a thorough understanding of the graphene/IL interface [30]. However, only a few reports focused on the influence of the graphene on the VS for ILs using DFT calculation. Comparing with the MD simulation, DFT calculation can investigate the VS of ILs systems more precisely on the microscopic scale. Under these circumstances, the VS for ILs on the graphene systems need to be investigated using DFT calculation. In this study, we performed a DFT calculation to investigate the influence of the graphene on the VS of imidazolium-based IL 1-Ethyl-3-methylimidazolium tetrafluoroborate ([Emim][$BF_4$]) in the range from 10 to 3500 $cm^{-1}$ at room temperature. Firstly, we calculated the VS of [Emim][$BF_4$] in the range from 10 to 3500 $cm^{-1}$ and found the main features of the experimentally measured spectrum are reproduced by the calculated VBs using DFT calculation. Secondly, the VS of [Emim][$BF_4$] on graphene surface in the range from 10 to 3500 $cm^{-1}$ was also calculated using DFT calculation. Finally, the influence of graphene on the position of VS of [Emim][$BF_4$] was investigated. In particular, we found that graphene not only changed the position of VS, but also enhance some vibrational bands in the range from 10 to 300 $cm^{-1}$.

## 2. Computations

To find the most stable structures of [Emim][$BF_4$] pair, there are 20 structures were generated using the Molclus program [31] which were adopted as initial structures for quantum chemistry optimization at B3LYP-D3/TZVP [32–34] level using Gaussian09 program [35]. The comparing of data obtained from the DFT calculations with the experimental data of vibrational spectrum of [Emim][$BF_4$] is presented in Table S1, and B3LYP-D3/TZVP calculation level is selected in this study. The initial geometries were generated randomly by the genmer and gentor tool in the Molclus package. After optimization by Gaussian09, six kinds of structures were obtained by energy using Molclus, and none of them have imaginary frequency. The lowest energy of [Emim][$BF_4$] pair is −768.740207 hartree, and the energy differences between the six structures and the most stable structure is 0, 0.74, 0.96, 1.17, 1.50 and 8.53 kcal·$mol^{-1}$, respectively, as showed in Fig. 1(The related coordinate files are listed in Supporting information).

Then the most stable structure of [Emim][$BF_4$] was used to combine with the graphene for optimization and frequency calculation by Gaussian09 program at B3LYP-D3/TZVP level, before that, the graphene and [Emim][$BF_4$] were already employed optimization and frequency calculation at B3LYP-D3/TZVP level and they did not show imaginary frequency. The relative positions of graphene and [Emim][$BF_4$] ion pairs were judged by electrostatic surfaces potential (ESP) of molecule calculated by Multiwfn program [36] and displayed by VMD software [37], and the ESP are showed in Fig. 2. The red and blue isosurface represent

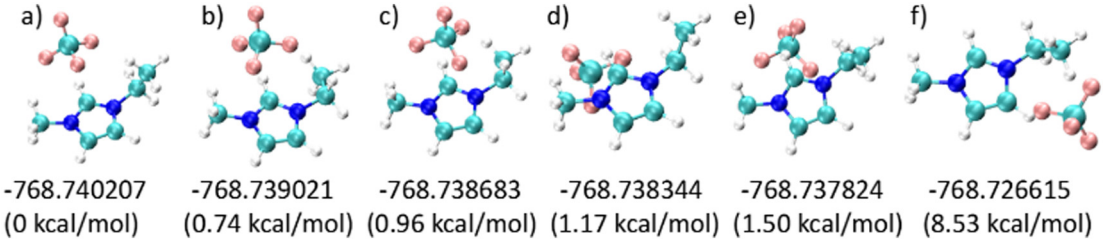


**Fig. 1.** Six kinds of stable [Emim][$BF_4$] structures. The B3LYP-D3/TZVP (Hartree) electronic energies and their relative energies to the global-minimum energy (in parenthesis). The most stable structure is (a) (The energy difference is small in the unit of hartree, so keep six decimals and convert the energy difference to kcal·$mol^{-1}$).

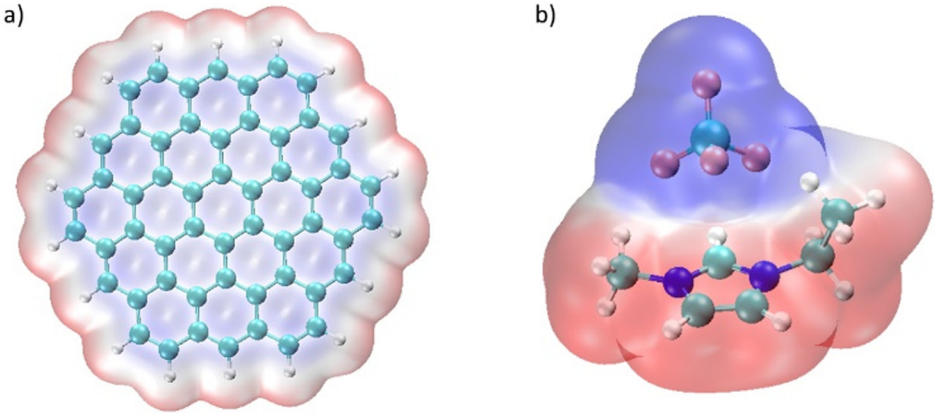


**Fig. 2.** (a) ESP of graphene, (b) ESP of [Emim][$BF_4$]. The red and blue isosurface represent the areas with positive and negative electrostatic potentials respectively.

the regions where the electrostatic potential is positive and negative respectively. The positive and negative electric potential should be complementary to make the binding of graphene and [Emim][$BF_4$] ion pair more stable, so the cation is closer to graphene than anion and the imidazole ring of $[Emim]^+$ was placed almost parallel to the graphene surface as the initial structure for optimization and frequency calculation of g-[Emim][$BF_4$]. Last, the vibrational peaks were classified through gaussview program [38] and the corresponding vibrational modes were compared one by one.

## 3. Results and discussion

### 3.1. Structure of complex and vibrational spectra

The optimized structures of [Emim][$BF_4$] and the system containing graphene and [Emim][$BF_4$] (g-[Emim][$BF_4$]) are shown in Fig. 3. From the molecular model in Fig. 3, it is found that the anion tetrafluoroborate ($[BF_4]^-$) of g-[Emim][$BF_4$] have changed its position relative to the cation $[Emim]^+$ compared to isolated [Emim][$BF_4$] ion pair, while the $[BF_4]^-$ of g-[Emim][$BF_4$] was almost on one side of C2—H and further away from the imidazole ring.

In order to further explain why the anion $[BF_4]^-$ have changed the position relative to cation $[Emim]^+$ in g-[Emim][$BF_4$], the independent gradient model (IGM) [39] was used to show the weak interaction among the fragments in g-[Emim][$BF_4$] system, and the weak interaction among the fragments are showed in Fig. 4. The position of anion relative to cation changed due to the interaction dominated by dispersion between graphene surface and [Emim][$BF_4$]. The change in the strength of the interaction between the ions of [Emim][$BF_4$] and the shift of the vibrational peak are exactly caused by [Emim][$BF_4$] absorbed on graphene surface.

The assignment of vibrational bands of [Emim][$BF_4$] and g-[Emim][$BF_4$] (the same vibration of [Emim][$BF_4$] and g-[Emim][$BF_4$] listed in Table S2, and all kinds vibration of g-[Emim][$BF_4$] listed in Table S3) which have significant changes was listed in Table 1 and the vibrational frequency all has been scaled by correction factor of 0.965 [40]. Details of the vibrational spectra and the vibrational bands assigning are given in Table 1 and Fig. 5. It can be seen that the frequency of different

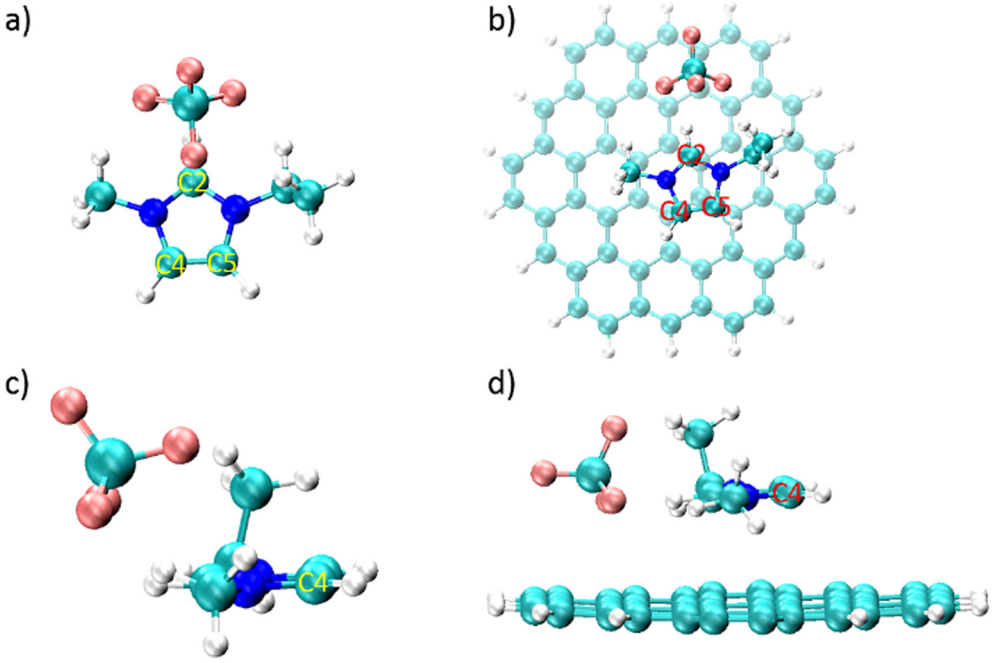


**Fig. 3.** The structures of [Emim][$BF_4$] and g-[Emim][$BF_4$]. (a) top view of [Emim][$BF_4$], (b) top view of g-[Emim][$BF_4$], (c) a side view of [Emim][$BF_4$], (d) a side view of g-[Emim][$BF_4$].

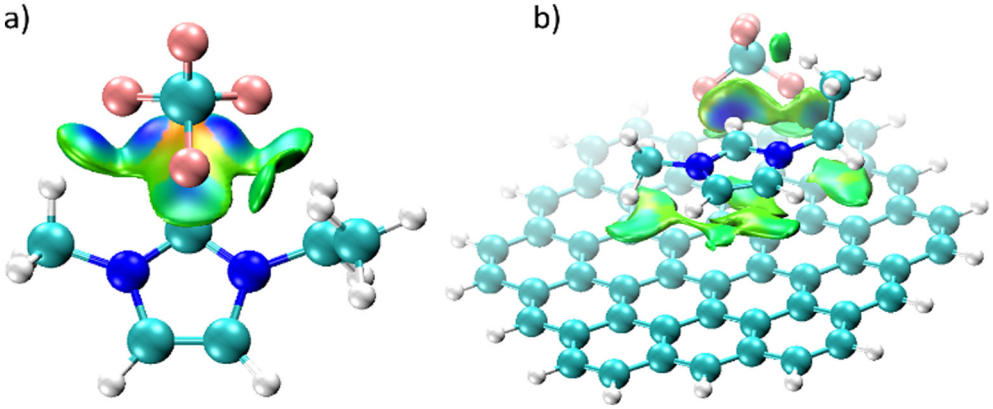


**Fig. 4.** Schematic diagram of weak interaction between fragments. (a) schematic diagram of weak interaction between $[Emim]^+$ and $[BF_4]^-$, (b) schematic diagram of weak interaction between fragments in g-[Emim][$BF_4$] system. Blue regions represent weak interactions that are strong and attractive, such as HBs, and the green regions represent very weak interactions, such as van der Waals, and red or orange regions represent repulsive effects between atoms.

**Table 1**
The assignment of part vibrational bands of [Emim][$BF_4$] and g-[Emim][$BF_4$].

| [Emim][$BF_4$] | | g-[Emim][$BF_4$] | | Assignments | Shift ($cm^{-1}$)[a] |
|---|---|---|---|---|---|
| $\nu$($cm^{-1}$) | I | $\nu$($cm^{-1}$) | I | | |
| 86.91 | 8.82 | 27.48 | 2.32 | $BF_4$ rotation,Emim rotation | −59.43 |
| 101.49 | 0.81 | 163.91 | 1.77 | δtwist $CH_3$(Me) | 62.43 |
| 126.40 | 14.75 | 142.04 | 1.98 | δtwist $CH_3$(Me),δr $CH_2$-$CH_3$ | 15.64 |
| 232.44 | 1.51 | 239.81 | 2.99 | δwag N-Me | 7.37 |
| 377.89 | 1.93 | 391.01 | 0.30 | δs Me-N3-C2H,δs $CH_3$-$CH_2$-N1 | 13.11 |
| 424.45 | 0.97 | 410.27 | 0.45 | δs Et-N1-C2H,Me-N3-C2H | −14.18 |
| 816.36 | 0.10 | 822.58 | 3.11 | δwag C4H,C5H | 6.21 |
| 882.46 | 86.77 | 896.96 | 11.92 | δwag C2-H | 14.50 |
| 952.68 | 272.75 | 941.90 | 46.92 | $\nu$ $BF_4$,δr C2-H | −10.78 |
| 975.22 | 264.54 | 1003.02 | 509.52 | $\nu$ $BF_4$,δwag C2-H | 27.80 |
| 1070.20 | 9.18 | 1078.33 | 6.67 | δwag $CH_3$(Me),δtwist $CH_2$ | 8.13 |
| 1145.49 | 519.17 | 1125.99 | 244.49 | δr C2H,C5H,$\nu$ $BF_4$ | −19.50 |
| 1336.15 | 5.78 | 1343.75 | 1.90 | δwag $CH_2$,δwag $CH_3$(Me) | 7.60 |
| 1402.15 | 2.79 | 1416.11 | 5.20 | δs $CH_3$(Me) | 13.95 |
| 1417.43 | 9.16 | 1441.30 | 21.53 | δas $CH_3$(Me) | 23.86 |
| 1455.58 | 13.77 | 1460.76 | 0.39 | δas $CH_3$(Me) | 5.18 |
| 1457.92 | 6.66 | 1463.47 | 5.76 | δas $CH_3$(Me) | 5.55 |
| 2939.26 | 12.52 | 2932.29 | 21.96 | $\nu$s $CH_3$(Et) | −6.98 |
| 2955.87 | 12.52 | 2964.72 | 10.35 | $\nu$s $CH_3$(Me) | 8.85 |
| 2963.32 | 12.52 | 2989.43 | 6.16 | $\nu$s $CH_2$ | 26.10 |
| 3033.51 | 12.52 | 3018.56 | 2.57 | $\nu$as $CH_3$(Et),$\nu$s $CH_2$ | −14.95 |
| 3034.01 | 12.52 | 3040.14 | 2.05 | $\nu$as $CH_3$(Me) | 6.13 |
| 3043.80 | 0.70 | 3060.88 | 0.15 | $\nu$as $CH_2$ | 17.08 |
| 3054.38 | 11.68 | 3066.08 | 0.39 | $\nu$as $CH_3$(Me) | 11.71 |
| 3170.26 | 97.67 | 3110.79 | 126.76 | $\nu$ C2-H | −59.46 |

[a] The shift is the vibrational frequency variation of vibrational peak frequency in [Emim][$BF_4$] relative to the same vibrational peak in g-[Emim][$BF_4$], that is, the frequency of corresponding vibration in g-[Emim][$BF_4$] is subtracted from the frequency in [Emim][$BF_4$] for the same vibration.

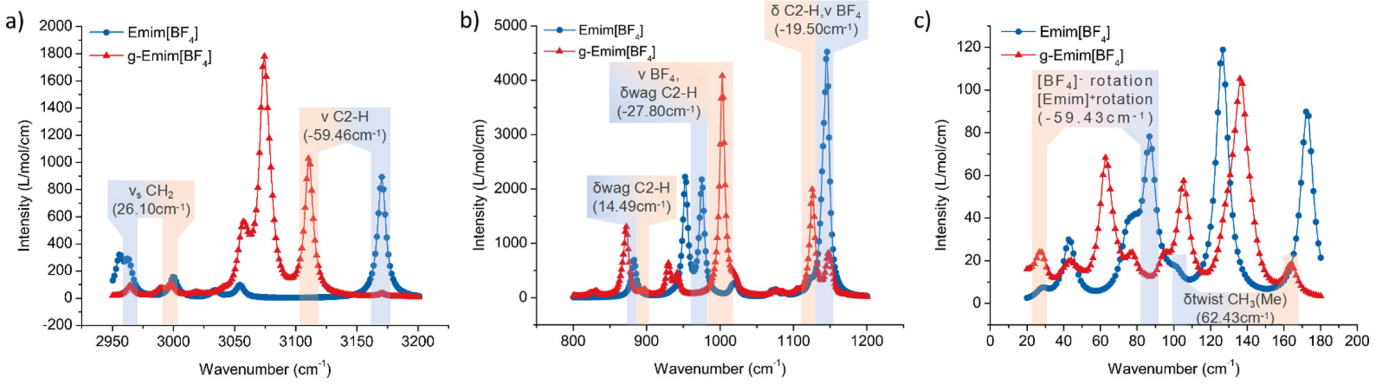


**Fig. 5.** Vibration spectra of [Emim][$BF_4$] and g-[Emim][$BF_4$]. (a) The vibration peaks with obvious shift between 2900 and 3200 $cm^{-1}$ are indicated on the spectra, (b) the vibration peaks with obvious shift between 800 and 1200 $cm^{-1}$ are indicated on the spectra, (c) the vibration peaks with obvious shift between 20 and 180 $cm^{-1}$ are indicated on the spectra.

vibration modes of the same functional group varies in the case of redshift or blueshift. Further analysis shows that the influence of the same reason on the shift of different vibration peaks is different. For example, the vibrational peaks of the wagging vibration and rocking vibration of C2—H bond at 882.46 and 3170.26 $cm^{-1}$ show a blueshift of 14.50 $cm^{-1}$ and redshift 59.46 $cm^{-1}$ respectively, these shifts are dominated by the change of HBs strength in [Emim][$BF_4$]. However, the vibrational peaks of the stretching or bending vibration of methyl or methylene all show a blueshift, such as the vibrational peak at 101.49, 1417.43 and 2963.32 $cm^{-1}$ show a blueshift of 62.43, 23.86 and 26.10 $cm^{-1}$ respectively. The rotation vibration of anion and cation at 86.91 $cm^{-1}$ and the wagging vibration of C4—H and C5—H at 816.36 $cm^{-1}$ show a redshift of 59.43 $cm^{-1}$ and blueshift of 6.21 $cm^{-1}$ respectively, which was dominated by the decrease of the interaction energy between the anion and cation. The above three factors are the primary causes for the shift of the vibrational peak of [Emim][$BF_4$] on graphene. Next, we will analyze how these changes affect the vibrational peak of [Emim][$BF_4$] in details.

### 3.2. Influence of HB strength variation

In vibrational frequency of [Emim][$BF_4$], the wagging vibration of C2—H at 882.46 $cm^{-1}$, rocking vibration of C2—H at 1145.49 $cm^{-1}$ and stretching vibration of C2—H at 3170.26 $cm^{-1}$ have changed which were mainly caused by the strength of HB C2-H···F. As can be seen from Fig. 3, the position of anion $[BF_4]^-$ relative to cation $[Emim]^+$ have changed. Compared with the isolated [Emim][$BF_4$] pair, the distance between F1 atom and H atom on C2—H in the ion pair of g-[Emim][$BF_4$] is closer. Fig. 6 shows that the distance between F1 atom and H atom on C2—H decreases from 2.214 to 1.897 Å, and the HB angle of C2-H···F1 increases from 120.49 to 161.75°. Meanwhile, the distance between F2 atom and H atom on C2—H increases from 2.195 to 2.325 Å, and the HB angle of C2-H···F2 increases from 120.79 to 132.59°. From the above, the HB C2-H···F1 significantly enhances and C2-H···F2 slightly weakens. Overall, HB between C2—H and anion enhances. Meanwhile, the attraction to hydrogen atom on C2—H enhances, and the length of C2—H is slightly increased from 1.076 to

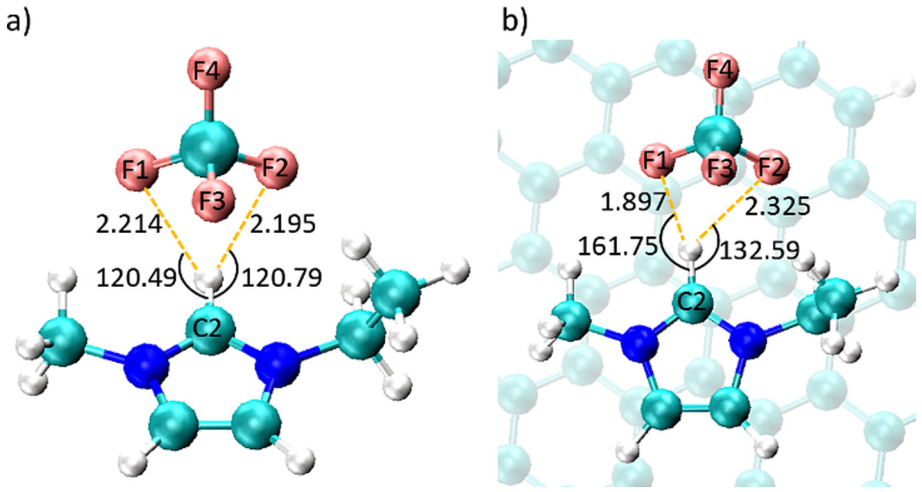


**Fig. 6.** C2-H···F HB of [Emim][$BF_4$] and g-[Emim][$BF_4$]. (a) The C2-H···F HB of [Emim][$BF_4$], (b) the C2-H···F HB of [Emim][$BF_4$] on graphene surface.

1.079 Å, so the vibration of C2—H wagging vibration at 882.46 $cm^{-1}$, rocking vibration at 1145.49 $cm^{-1}$ and stretching vibration at 3170.26 $cm^{-1}$ show a blueshift of 14.50 $cm^{-1}$, redshift of 19.50 $cm^{-1}$ and 59.43 $cm^{-1}$ respectively. Therefore, the shift of stretching vibration, rocking vibration and wagging vibration of C2—H was mainly caused by the change of HB strength between ions.

It can be seen that the rocking vibration of C2—H bond at 1145.49 $cm^{-1}$, besides the vibration of C2—H bond, it is also accompanied by the stretching vibration of B—F. According to the above-mentioned analysis, C2—H···F1 HB significantly enhances, while C2—H···F2 HB slightly weakens. Thus, the length of B—F1 bond obviously increases from 1.429 to 1.437 Å, while the length of B—F2 bond mildly reduces from 1.428 to 1.425 Å as shown in Table 2. So the stretching vibration of B—F at 1145.49 $cm^{-1}$ shows a redshift and at 952.68 $cm^{-1}$ is the same as it. This vibrational peak represents the stretching vibration of B—F1 and B—F2, and shows a redshift of 10.78 $cm^{-1}$ precisely because the change of C2—H···F HB strength.

However, due to the change of relative position between anion and cation, not only the C2-H···F HB strength changed, but also the interaction between B—F3 and imidazole ring significantly weakens as shown in the Fig. 4. As showed in Fig. 7, the interaction between B—F3 and cation of [Emim][$BF_4$] is dominated by strong attraction between B—F3 and imidazole ring and HB between C—H and F3 of methyl group of the ethyl chain (C7-H···F3). However, the interaction between B—F3 and cation in g-[Emim][$BF_4$] is only dominated by C7—H···F3 HB. So F3 atom is more attractive to H atom forming HB qualitatively, although C7-H···F3 seems to be weakened from the Fig. 7, but it is not true. From the data in Table 2, we can also see that the length of C—H bond forming HB with F3 is extended from 1.089 to 1.090 Å and the bond length of other C—H bond of methyl group on the ethyl chain are also elongated. So that the bending and stretching vibration of methyl on ethyl chain at 2939.26 and 3033.51 $cm^{-1}$ shows a redshift of 6.98 and 14.95 $cm^{-1}$ respectively. The vibrational peak at 3033.51 $cm^{-1}$ not only contains the stretching vibration of C7—H, but also is accompanied by the stretching vibration of C—H of methylene on the ethyl chain, corresponding to the C6-H1 bond in Fig. 7. It can be seen from Fig. 7 that the HB C6-H1···F2 enhances, so the stretching vibration of C6-H1 at 3033.51 $cm^{-1}$ shows a redshift. Hence the attraction between anion and ethyl chain is more obvious, so the bending vibration of the N1—C (Et) at 424.45 $cm^{-1}$ shows a redshift of 14.18 $cm^{-1}$ to 410.27 $cm^{-1}$. But the same explanation doesn't work on the vibrational peak of methylene expect at 3033.51 $cm^{-1}$, because the other vibrational peaks of methylene always almost show blueshift, which was caused by the enhanced induction effect between anion and cation. The influence of graphene on the induction effect between ions was analyzed later.

**Table 2**
Bond length of [Emim][$BF_4$] (Å).[a]

| Bond | [Emim][$BF_4$] | G-[Emim][$BF_4$] | △ |
|---|---|---|---|
| C2-H | 1.076 | 1.079 | 0.004 |
| H···B | 1.075 | 1.074 | 0.000 |
| N-Me | 1.074 | 1.074 | 0.000 |
| N-Et | 2.494 | 2.370 | −0.124 |
| N1-C2 | 1.464 | 1.463 | −0.001 |
| C2-N3 | 1.475 | 1.477 | 0.001 |
| N3-C4 | 1.332 | 1.333 | 0.002 |
| C4 = C5 | 1.333 | 1.335 | 0.002 |
| C5-N1 | 1.383 | 1.384 | 0.002 |
| $CH_2$(Et) | 1.357 | 1.358 | 0.001 |
| | 1.383 | 1.384 | 0.001 |
| $CH_3$(Et) | 1.087 | 1.085 | −0.001 |
| | 1.091 | 1.088 | −0.002 |
| | 1.089 | 1.090 | 0.002 |
| $CH_3$(Me) | 1.092 | 1.092 | 0.000 |
| | 1.091 | 1.091 | 0.000 |
| | 1.088 | 1.086 | −0.001 |
| B-F1 | 1.087 | 1.089 | 0.002 |
| B-F2 | 1.089 | 1.086 | −0.003 |
| B-F3 | 1.429 | 1.437 | 0.008 |
| B-F4 | 1.428 | 1.425 | −0.003 |

[a] The data in the table are only three decimal places, and the change of bond length was calculated by the original data with five decimal places, so some differences seem to be inconsistent with the values directly calculated in the table.

### 3.3. Influence of interaction energy variation

We used DFT-symmetry adapted perturbation theory (SAPT(DFT)) which is an extension of the SAPT, through PSI4 program [41] at aug-cc-pvdz calculation level to decompose the interaction energy between the anion and cation of the [Emim][$BF_4$] ion pair while the [Emim][$BF_4$] ion pair is isolated or placed on graphene surface. The interaction energy between graphene and [Emim][$BF_4$], anion or cation are also decomposed. The components of the interaction energy are shown in Table 3. Compared with the [Emim][$BF_4$] ion pair in isolation, the interaction energy between anion and cation of the [Emim][$BF_4$] ion pair on graphene surface reduces from −367.02 to −356.06 kJ $mol^{-1}$. We can also find that the weak interaction between graphene and [Emim][$BF_4$] ion pair is dominated by dispersion interaction from the energy components data in Table 3. The induction and dispersion interaction accounts for 63.43% and 34.37% of the attraction between graphene and the anion $[BF_4]^-$ respectively ($E_{Dis}\% = E_{Dis}/E_{Attr}(tot)$ [42]), which have dominated the anion closer to the surface of graphene.

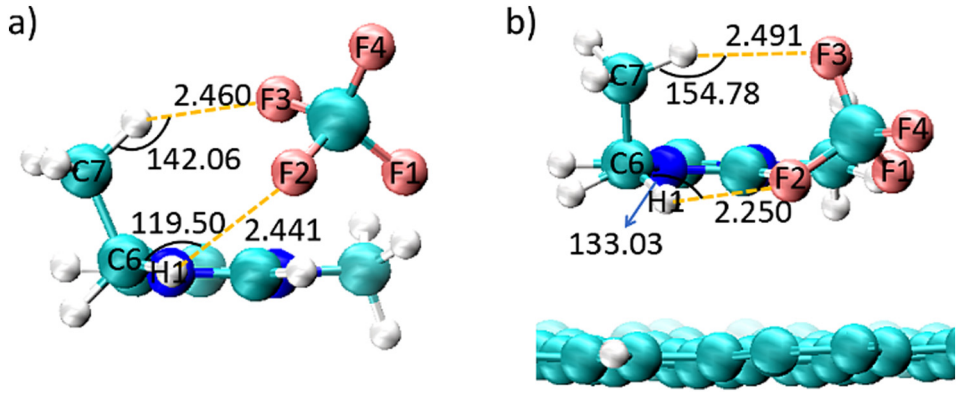


**Fig. 7.** C7-H···F3 and C6-H···F2 HB of [Emim][$BF_4$] and g-[Emim][$BF_4$]. (a) C7-H···F3 and C6-H···F2 HB of [Emim][$BF_4$], (b) C7-H···F3 and C6-H···F2 HB of [Emim][$BF_4$] on graphene surface. Bond lengths in Å, bond angles in degrees.

**Table 3**
The energy component of the interaction energy (kJ $mol^{-1}$).

| (kJ·$mol^{-1}$) | Electrostatics | Exchange | Induction | delta HF,r (2) | Dispersion | Total SAPT(DFT) |
|---|---|---|---|---|---|---|
| Emim[$BF_4$] | −383.28 | 93.72 | −44.72 | −11.53 | −32.74 | −367.02 |
| Emim[$BF_4$](G) | −360.32 | 74.73 | −45.42 | −12.15 | −25.04 | −356.06 |
| G-Emim[$BF_4$] | −36.43 | 88.91 | −28.96 | −8.11 | −99.24 | −75.72 |
| G-Emim | −57.24 | 66.94 | 12.23 | −6.75 | −76.86 | −54.94 |
| G-[$BF_4$] | 20.81 | 21.97 | −41.19 | −1.36 | −22.38 | −20.78 |

Because the interaction energy of [Emim][$BF_4$] ion pair decreased in g-[Emim][$BF_4$], so the interaction between the anion $[BF_4]^-$ and the hydrogen atoms attached to C4 and C5 atoms also decreased. Therefore, the wagging vibrational frequency of C4—H and C5—H increased, that is, the wagging vibrational frequency of C4—H and C5—H of [Emim][$BF_4$] ion pair show a blueshift of 6.21 $cm^{-1}$ from 816.36 to 822.58 $cm^{-1}$.The vibrational frequency of rotational vibration of anion and cation at 86.91 $cm^{-1}$ shows a redshift of 59.43 $cm^{-1}$ in g-[Emim][$BF_4$], that was also caused by the decrease of the [Emim][$BF_4$] ion pair interaction energy in g-[Emim][$BF_4$]. This is because the interaction energy between anion and cation decreases, and the rotational vibration frequency of anion and cation decreases. As the interaction energy between ions decreased, the attraction of anion to methyl decreased, which can also be seen in Fig. 4. So the bending vibration of N3-C(Me) bond at 377.89 $cm^{-1}$ and the wagging vibration of N3-C(Me) at 232.44 $cm^{-1}$ show a blueshift of 13.11 and 7.37 $cm^{-1}$ respectively.

The stretching vibrational peak of B—F bond at 975.22 $cm^{-1}$ shows a blueshift of 27.80 $cm^{-1}$. This vibrational peak can be assigned as the strong stretching vibration of B—F3 and the weak stretching vibration of B—F1 and B—F2. As showed in Fig. 4, the attraction between F3 and imidazole ring in g-[Emim][$BF_4$] significantly weakens, which is manifestation of reduced interaction energy between anion and cation. Hence the attraction to B—F3 bond significantly weakens. Compared with isolated [Emim][$BF_4$], the length of B—F3 bond in g-[Emim][$BF_4$] shortens from 1.422 to 1.407 Å, and that is exactly why the vibrational peak at 975.22 $cm^{-1}$ shows a blueshift 27.80 $cm^{-1}$.

### 3.4. Influence of inductive effect variation

It can be seen that the vibrational bands which have significantly shift is mostly related to the vibration of methyl and methylene on cation, and the relevant vibrational bands almost all shows a blueshift in g-[Emim][$BF_4$]. As shown in Table 1, the vibrational peaks at 101.49, 126.40, 1070.20, 1336.15, 1402.15, 1417.43, 1455.58, 1457.92, 2955.87, 2963.32, 3034.01, 3043.80, 3054.38 $cm^{-1}$ in [Emim][$BF_4$] are the stretching or bending vibration of methyl or methylene groups, which show a blueshift of 62.43, 15.64, 8.13, 7.60, 13.95, 23.86, 5.18, 5.55, 8.85, 26.10, 6.13, 17.08, 11.71 $cm^{-1}$ respectively in g-[Emim][$BF_4$]. This is due to an increased induction effect on the alkyl chain which leads to the charge distribution on the alkyl chain changed, it can also be verified in the components obtained by energy decomposition (Table 3) that an increase of 0.70 kJ $mol^{-1}$ in the induced energy in g-[Emim][$BF_4$] compared to the isolated [Emim][$BF_4$]. Because of the π-π stacking between graphene and the cation, the charge distribution on the imidazole ring is changed, which further affected the charge distribution on the alkyl chain. It can be seen from Table 4 that the charge amount of methylene group on the ethyl chain and methyl significantly changed, absorbing −0.097 and −0.065 a.u electrons respectively, so the vibrational frequency of these groups shows blueshift. Meanwhile, it can be seen from Table 2 that the bond length of C—H on methyl and methylene group shortens in different degrees, which corresponds to blueshift of these vibrational peaks. From Table 4, we can see that the charge of methyl group on the ethyl chain also slightly changed, absorbing −0.006 a.u electrons, but its vibrational peak mostly shows a redshift, because the change of HB strength plays a leading role in the vibration of this methyl, as analyzed before.

Actually, the shift of vibrational peak of [Emim][$BF_4$] is the result of many effects. For a specific vibrational peak, the dominate factor that causes the shift is different, while for the same factor, different vibrational peak have different shift.

**Table 4**
Charge information of fragment of [Emim][$BF_4$]and g-[Emim][$BF_4$].[a]

| | [Emim][$BF_4$] | g-[Emim][$BF_4$] | △ |
|---|---|---|---|
| [Emim][$BF_4$] | 0.000 | −0.062 | −0.062 |
| $[Emim]^+$ | 0.778 | 0.691 | −0.087 |
| $[BF_4]^-$ | −0.778 | −0.753 | 0.025 |
| $CH_2$ | 0.186 | 0.121 | −0.065 |
| $CH_3$(Et) | 0.057 | 0.051 | −0.006 |
| $CH_3$(Me) | 0.289 | 0.192 | −0.097 |

[a] △ means the electric charge difference between g-[Emim][$BF_4$] and [Emim][$BF_4$], the unit of charge in this paper is a.u.

## 4. Conclusions

In this study, we investigated the influence of graphene on the vibrational bands of [Emim][$BF_4$] and systematically analyzed the internal reasons for the significant change of [Emim][$BF_4$] VBs. The research results show that it was mainly caused by the change of the HB strength, interaction energy induction effect of [Emim][$BF_4$] ion pair. Further analysis shows that the interaction between graphene surface and [Emim][$BF_4$] ion pair was dominate by dispersion, it is precise because the position of anion $[BF_4]^-$ relative to cation $[Emim]^+$ have changed to this interaction, that is why this series of VBs changes happened. It can be seen that the result of the synergy of these factors leads to vibrational peak shift obviously. This paper analyzes the effect of graphene on ILs VS, which is of great significance for exploring the interaction mechanism between graphene and ILs.

## CRediT authorship contribution statement

**Jiao Zhang:** Conceptualization, Methodology, Validation, Formal analysis, Investigation, Writing - original draft, Visualization. **Yongji Guan:** Conceptualization, Methodology, Formal analysis, Writing - review & editing, Project administration, Funding acquisition .**Jinyuan Wang:** Software. **Fulong Yang:** Resources. **Huanwang Jing:** Software. **Xiaoping Zhang:** Resources, Supervision, Funding acquisition. **Youquan Deng:** Resources, Supervision, Funding acquisition.

## Declaration of competing interest

The authors declare that they have no known competing financial interests or personal relationships that could have appeared to influence the work reported in this paper.

## Acknowledgements

The authors acknowledge the financial support of this work from the National Key Research and Development Program of China (2017YFA0403101), the Lanzhou University International Teacher Postdoctoral Scholarship Fund, the Fundamental Research Funds for the Central Universities (lzujbky-2018-it62 and lzujbky-2018-127) and the National Natural Science Foundation of China (61804071).

## Appendix A. Supplementary data

Supplementary data to this article can be found online at https://doi.org/10.1016/j.molliq.2020.113340.

## References

[1] M. Falk, T. Ford, Can. J. Chem. 44 (14) (1966) 1699–1707.
[2] P.L. Silvestrelli, M. Bernasconi, M. Parrinello, Chem. Phys. Lett. 277 (5–6) (1997) 478–482.
[3] C. Zhang, D. Donadio, F. Gygi, G. Galli, J. Chem. Theory Comput. 7 (5) (2011) 1443–1449.
[4] C.F. Poole, B.R. Kersten, S.S. Ho, M.E. Coddens, K.G. Furton, J. Chromatogr. A 352 (1986) 407–425.
[5] P.H. Shetty, P.J. Youngberg, B.R. Kersten, C.F. Poole, J. Chromatogr. A 411 (1987) 61–79.
[6] P. Wasserscheid, W. Keim, Angew. Chem. Int. Ed. 39 (21) (2000) 3772–3789.
[7] T. Welton, Chem. Rev. 99 (8) (1999) 2071–2084.
[8] J.G. Huddleston, A.E. Visser, W.M. Reichert, H.D. Willauer, G.A. Broker, R.D. Rogers, Green Chem. 3 (4) (2001) 156–164.
[9] J. Dupont, R.F. de Souza, P.A. Suarez, Chem. Rev. 102 (10) (2002) 3667–3692.
[10] J.H. Davis Jr., P.A. Fox, Chem. Commun. (11) (2003) 1209–1212.
[11] K.R. Seddon, Nat. Mater. 2 (6) (2003) 363.
[12] R. Sheldon, Chem. Commun. (23) (2001) 2399–2407.
[13] C.M. Gordon, Appl. Catal. A Gen. 222 (1–2) (2001) 101–117.
[14] K.E. Gutowski, G.A. Broker, H.D. Willauer, J.G. Huddleston, R.P. Swatloski, J.D. Holbrey, R.D. Rogers, J. Am. Chem. Soc. 125 (22) (2003) 6632–6633.
[15] P. Hapiot, C. Lagrost, Chem. Rev. 108 (7) (2008) 2238–2264.
[16] M. Galiński, A. Lewandowski, I. Stępniak, Electrochim. Acta 51 (26) (2006) 5567–5580.
[17] X. He, Q. Shao, P. Cao, W. Kong, J. Sun, X. Zhang, Y. Deng, Lab Chip 15 (5) (2015) 1311–1319.
[18] X. Hu, S. Zhang, C. Qu, Q. Zhang, L. Lu, X. Ma, X. Zhang, Y. Deng, Soft Matter 7 (13) (2011) 5941–5943.
[19] W. Kong, L. Cheng, X. He, Z. Xu, X. Ma, Y. He, L. Lu, X. Zhang, Y. Deng, Microfluid. Nanofluid. 18 (5–6) (2015) 1299–1307.
[20] Q. Shao, J. Jia, Y. Guan, X. He, X. Zhang, J. Chem. Phys. 144 (12) (2016), 124703. .
[21] Y. Guan, Q. Shao, W. Chen, J. Zhang, X. Zhang, Y. Deng, J. Mater. Chem. A 6 (25) (2018) 11941–11950.
[22] Y. Guan, W. Chen, J. Zhang, F. Yang, C. Du, X. Zhang, Y. Deng, J. Phys. Chem. C 123 (12) (2019) 6981–6988.
[23] Y. Guan, Q. Shao, W. Chen, S. Liu, X. Zhang, Y. Deng, J. Phys. Chem. C 121 (42) (2017) 23716–23726.
[24] X. Hu, S. Zhang, Y. Liu, C. Qu, L. Lu, X. Ma, X. Zhang, Y. Deng, Appl. Phys. Lett. 99 (21) (2011) 213505.
[25] K. Fumino, V. Fossog, P. Stange, K. Wittler, W. Polet, R. Hempelmann, R. Ludwig, ChemPhysChem 15 (12) (2014) 2604–2609.
[26] G. Velpula, R. Phillipson, J.X. Lian, D. Cornil, P. Walke, K. Verguts, S. Brems, H. Uji-i, S. De Gendt, D. Beljonne, ACS Nano 13 (3) (2019) 3512–3521.
[27] A.S. Pensado, F. Malberg, M.C. Gomes, A.A. Padua, J. Fernández, B. Kirchner, RSC Adv. 4 (35) (2014) 18017–18024.
[28] Y. Chen, X. Zhang, D. Zhang, P. Yu, Y. Ma, Carbon 49 (2) (2011) 573–580.
[29] S. Vivekchand, C.S. Rout, K. Subrahmanyam, A. Govindaraj, C. Rao, J. Chem. Sci. 120 (1) (2008) 9–13.
[30] G. Feng, S. Li, V. Presser, P.T. Cummings, J. Phys. Chem. Lett. 4 (19) (2013) 3367–3376.
[31] T. Lu, Molclus program, version 1.8, http://www.keinsci.com/research/molclus.html.
[32] A. Schäfer, C. Huber, R. Ahlrichs, J. Chem. Phys. 100 (8) (1994) 5829–5835.
[33] C. Lee, W. Yang, R. Parr, J. Phys. Chem. 98 (1994) 11623.
[34] S. Grimme, J. Antony, S. Ehrlich, H. Krieg, J. Chem. Phys. 132 (15) (2010), 154104. .
[35] G.W.T.M.J. Frisch, H.B. Schlegel, G.E. Scuseria, M.A. Robb, J.R. Cheeseman, G. Scalmani, V. Barone, G.A. Petersson, H. Nakatsuji, X. Li, M. Caricato, A. Marenich, J. Bloino, B.G. Janesko, R. Gomperts, B. Mennucci, H.P. Hratchian, J.V. Ortiz, A.F. Izmaylov, J.L. Sonnenberg, D. Williams-Young, F. Ding, F. Lipparini, F. Egidi, J. Goings, B. Peng, A. Petrone, T. Henderson, D. Ranasinghe, V.G. Zakrzewski, J. Gao, N. Rega, G. Zheng, W. Liang, M. Hada, M. Ehara, K. Toyota, R. Fukuda, J. Hasegawa, M. Ishida, T. Nakajima, Y. Honda, O. Kitao, H. Nakai, T. Vreven, K. Throssell, J.A. Montgomery Jr., J.E. Peralta, F. Ogliaro, M. Bearpark, J.J. Heyd, E. Brothers, K.N. Kudin, V.N. Staroverov, T. Keith, R. Kobayashi, J. Normand, K. Raghavachari, A. Rendell, J.C. Burant, S.S. Iyengar, J. Tomasi, M. Cossi, J.M. Millam, M. Klene, C. Adamo, R. Cammi, J.W. Ochterski, R.L. Martin, K. Morokuma, O. Farkas, J.B. Foresman, D.J. Fox, Wallingford, CT, 2009.
[36] T. Lu, F. Chen, J. Comput. Chem. 33 (5) (2012) 580–592.
[37] W. Humphrey, A. Dalke, K. Schulten, J. Mol. Graph. 14 (1) (1996) 33–38.
[38] R. Dennington, T. Keith and J. Millam, Semichem Inc.: Shawnee Mission, KS (2009).
[39] C. Lefebvre, G. Rubez, H. Khartabil, J.-C. Boisson, J. Contreras-García, E. Hénon, Phys. Chem. Chem. Phys. 19 (27) (2017) 17928–17936.
[40] in NIST Computational Chemistry Comparison and Benchmark Database.
[41] R.M. Parrish, L.A. Burns, D.G. Smith, A.C. Simmonett, A.E. DePrince III, E.G. Hohenstein, U. Bozkaya, A.Y. Sokolov, R. Di Remigio, R.M. Richard, J. Chem. Theory Comput. 13 (7) (2017) 3185–3197.
[42] E.I. Izgorodina, D.R. MacFarlane, J. Phys. Chem. B 115 (49) (2011) 14659–14667.